

RESEARCH ARTICLE | MARCH 11 2025

Fano interference in single-molecule transistors

Yiping Ouyang; Rui Wang; Zewen Wu; Deping Guo; Yang-Yang Ju; Jun Chen ; Minhao Zhang ; Danfeng Pan ; Xuecou Tu ; Shuai Zhang ; Lin Kang ; Jian Chen ; Peiheng Wu ; Xuefeng Wang ; Jianguo Wan ; Wei Ji ; Xianghua Kong ; Yuan-Zhi Tan ; Fengqi Song

Check for updates

Appl. Phys. Lett. 126, 103102 (2025)

<https://doi.org/10.1063/5.0254457>



Articles You May Be Interested In

KoopmanLab: Machine learning for solving complex physics equations

APL Mach. Learn. (September 2023)

Experimental realization of a quantum classification: Bell state measurement via machine learning

APL Mach. Learn. (September 2023)

Nanotechnology & Materials Science


Optics & Photonics

Impedance Analysis

Scanning Probe Microscopy

Sensors


Failure Analysis & Semiconductors



Unlock the Full Spectrum.
From DC to 8.5 GHz.

Your Application. Measured.

[Find out more](#)



Fano interference in single-molecule transistors

Cite as: Appl. Phys. Lett. **126**, 103102 (2025); doi: [10.1063/5.0254457](https://doi.org/10.1063/5.0254457)

Submitted: 22 December 2024 · Accepted: 26 February 2025 ·

Published Online: 11 March 2025



View Online



Export Citation



CrossMark

Yiping Ouyang,^{1,2} Rui Wang,¹ Zewen Wu,³ Deping Guo,⁴ Yang-Yang Ju,⁵ Jun Chen,^{1,2} Minhao Zhang,^{1,2,a)} Danfeng Pan,⁶ Xuecou Tu,⁶ Shuai Zhang,^{1,2} Lin Kang,⁶ Jian Chen,⁶ Peiheng Wu,⁶ Xuefeng Wang,⁶ Jianguo Wan,¹ Wei Ji,^{4,a)} Xianghua Kong,^{3,a)} Yuan-Zhi Tan,^{5,a)} and Fengqi Song^{1,2,a)}

AFFILIATIONS

¹National Laboratory of Solid State Microstructures, Collaborative Innovation Center of Advanced Microstructures, and School of Physics, Nanjing University, Nanjing 210093, China

²Institute of Atom Manufacturing, Nanjing University, Suzhou 215163, China

³College of Physics and Optoelectronic Engineering, Shenzhen University, Shenzhen 518060, China

⁴Beijing Key Laboratory of Optoelectronic Functional Materials and Micro-Nano Devices, and Department of Physics, Renmin University of China, Beijing 100872, China

⁵State Key Laboratory of Physical Chemistry of Solid Surfaces, College of Chemistry and Chemical Engineering, Xiamen University, Xiamen 361005, China

⁶School of Electronic Science and Engineering and Collaborative Innovation Center of Advanced Microstructures, Nanjing University, Nanjing 210023, China

^{a)}Authors to whom correspondence should be addressed: zhangminhao@nju.edu.cn; wji@ruc.edu.cn; kongxianghuaphysics@szu.edu.cn; yuanzhi_tan@xmu.edu.cn; and songfengqi@nju.edu.cn

ABSTRACT

Quantum interference has been intensively pursued in molecular electronics to investigate and utilize coherent electron transport at the ultra-small level. An essential type of quantum interference with drastic destructive-constructive switching, known as Fano interference, has been widely reported in various kinds of nanoelectronics electronic systems, but not yet been electrostatically gating in a single-molecule device. Here, we fabricate the three-terminal single-molecule transistors based on the molecule with a long backbone and a side group to demonstrate the gate-controllable Fano interference. By applying bias and gate voltages, the two-dimensional differential conductance map shows the non-centrosymmetrical Fano patterns. Combined with the electron transport model and the first principles calculations, the resonant parameters of the Fano interference can unveil the coupling geometry of the junction and the spatial distribution of the resonant states. Our findings provide an instrumental method to induce and utilize the quantum interference behaviors at the molecular level.

© 2025 Author(s). All article content, except where otherwise noted, is licensed under a Creative Commons Attribution-NonCommercial-NoDerivs 4.0 International (CC BY-NC-ND) license (<https://creativecommons.org/licenses/by-nc-nd/4.0/>). <https://doi.org/10.1063/5.0254457>

Quantum interference (QI) at the molecular scale attracts considerable attention in terms of the quantum theories at the ultra-small scale and its practical utility in microelectronics.^{1–5} The control of QI has been demonstrated in various kinds of molecular electronics systems through the design of molecular structures,^{6–21} contact configurations,^{10–12} or electrical gating.^{12–18} The molecular structure determines the paths of electron transport, forming the basis of QI. The contact configuration to the electrodes influences the phase difference among electron paths, which is crucial for the effect of QI. The electrical field introduced by a gate can be used to tune the energy levels of molecular states, bringing with it the possibility of changing the phase difference that determines the status of QI.

Fano interference is a specific and essential type of QI that occurs between a discrete state and a continuous state.²² It is remarkable for its characteristic asymmetrical resonant profile and drastic destructive-constructive QI switching. Having been realized in many mesoscopic electronics devices,^{23–32} it is now highly sought after in molecular electronics, for the demonstration of a typical quantum effect and the potential applications in conductance controlling and thermoelectricity.^{4,5,17–21,32–40} The experimental feasibility of single-molecule electronic Fano interference has been proved by Zheng *et al.* using scanning tunneling microscopy.⁴¹ However, the lack of Fano asymmetrical factor q makes it confusing to understand some important details of the QI mechanism.^{34,38,39} This still awaits to be demonstrated in robust device-oriented single-molecule electronics.

The problems can be tackled in the single-molecule transistor (SMT) devices with the schematic as Fig. 1(a). The molecule consists of a long backbone anchored on the gold leads and an atomic group hanging on the side of the backbone. This configuration produces a quasi-continuous state on the backbone and a discrete state on the side group, which could induce Fano interference.^{42,43} The energy levels of the states can be tuned by the gate (V_g) and the bias (V_{sd}) voltages, making it feasible to manipulate the Fano interference and present the two-dimensional interference pattern.^{29,31}

Experimentally, it is hard to prepare such a device because it requires a well-designed molecular structure to produce the states and a well-controlled fabrication process to introduce an effective electrostatic field.^{40,44,45} We synthesize the 2,7-di(4-pyridyl)-9,9'-spirobifluorene (DPSBF) molecule and 2,7-di(pyridin-4-yl)-fluoren-9-one (DPFO)

molecule with nitrogen anchor sites on the terminals of the backbone to make this configuration possible in practical fabrication. The side groups in DPSBF and DPFO molecules provide the discrete states to join the Fano interference between the quasi-continuous backbone states. The devices are fabricated by feedback-controlled electromigration break junction (FCEBJ) technique.^{46,47} The process of the device fabrication is provided in Sec. 1 of the [supplementary material](#). Moreover, we combine the transport models of Fano interference in mesoscopic devices²⁷ and in molecular junctions³⁴ to obtain the Fano factor q , which is crucial to describe the features of the interfered states and the coupling configurations of the device. These features are all corroborated by the first principles calculations.

We perform experiments on 3 devices. Devices 1 and 2 are based on the DPSBF molecule, while device 3 is based on the DPFO molecule. Both molecules consist of a long backbone and a side group, but the side groups are different in each kind of molecule. In the main text, we mainly focus on device 1. The detailed results of devices 2 and 3 are shown in Sec. 5 of the [supplementary material](#).

Figure 1(b) shows the map of differential conductance ($G = dI_{sd}/dV_{sd}$, where I_{sd} is the bias current) of device 1 as the functions of V_g and V_{sd} at a fixed temperature 3 K. $G(V_g)$ curves extracted from the maps when $V_{sd} = 0$ is plotted in Fig. 1(c). The crossing patterns in the $G(V_g, V_{sd})$ maps and peaks in the zero-bias $G(V_g)$ curve manifest that we have accessed and manipulated the molecular orbitals.^{48,49} The obvious noncentrosymmetrical distributions in the $G(V_g, V_{sd})$ maps and the asymmetric shapes of the zero-bias $G(V_g)$ curves differ from ordinary symmetrical Coulomb Diamond phenomena but can be produced by Fano interference.^{29,31,50,51}

The transmission spectrum can be fitted by the Fano formula:^{22,25,31,52}

$$\tau(E) = A_F \frac{\left(\frac{E - \epsilon_F}{\Gamma_F/2} + q\right)^2}{\left(\frac{E - \epsilon_F}{\Gamma_F/2}\right)^2 + 1} + A_{BW} \frac{1}{\left(\frac{2(E - \epsilon_{BW})}{\Gamma_{BW}}\right)^2 + 1} + A_{off}. \quad (1)$$

It is a linear sum of an asymmetrical Fano resonant term, a symmetrical Breit-Wigner (BW) resonant term, and an off-resonant term, where A_F , A_{BW} , and A_{off} are the coefficients of the three terms; ϵ_F and ϵ_{BW} are the Fano and BW resonant levels, respectively; Γ_F and Γ_{BW} are the Fano and BW resonant widths, respectively; q is the Fano asymmetry factor. Based on Landauer formalism,⁵³ $\tau(E)$ gives an analytical solution of $G(V_g, V_{sd})$ at 0 K, in which $G(V_g, V_{sd})$ is also a linear sum of a Fano term, a BW term, and an off-resonant term [see Eq. (S6) in the [supplementary material](#)]. The optimal fitting parameters are listed in Table I.

The fitted $G(V_g, V_{sd})$ map in Fig. 1(d) and the zero-bias $G(V_g)$ curve in Fig. 1(e) exhibit the asymmetry consistent with the experimental ones. The Fano term of the zero-bias $G(V_g)$ curve has an asymmetric shape with a peak and a dip. Moreover, $q = 0.374$ corresponds to a more pronounced dip than the peak. We also observe such Fano interference patterns in devices 2 and 3, thus proving the reproducibility of this phenomenon. The fitting parameters of devices 2 and 3 are also listed in Table I, and their conductance data are provided in Sec. 5 of the [supplementary material](#).

The information in the table includes: The name of the molecule; the kind of the side group; the coefficients of terms in transmission

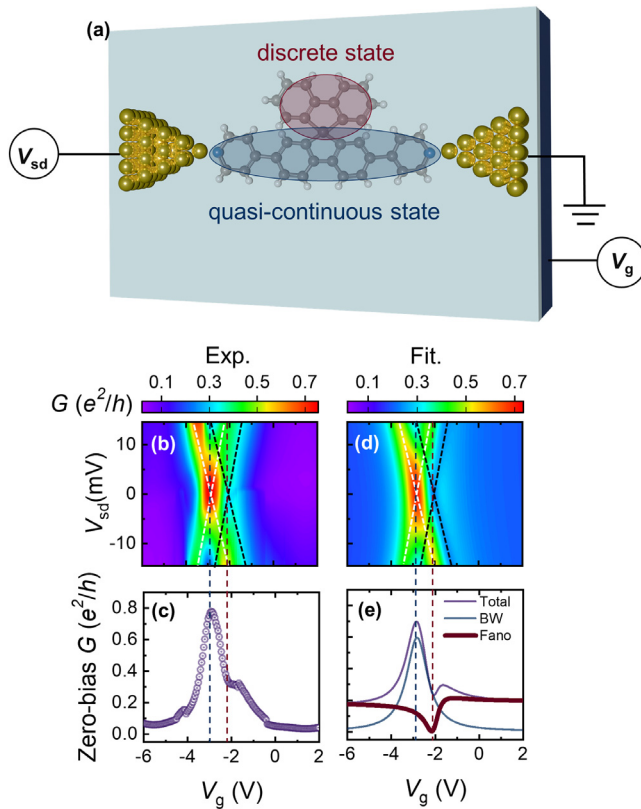


FIG. 1. Differential conductance pattern showing Fano resonance of device 1. (a) Schematic of the SMT device. The molecule has a long backbone anchored on the leads and an atomic group hanging on the side of the backbone, producing a quasi-continuous state and a discrete state to realize Fano interference. (b) Experimental differential conductance (G) maps plotted against the bias voltage V_{sd} and the gate V_g voltage of device 1 at temperature $T = 3$ K. (c) G - V_g curves extracted from (b) at $V_{sd} = 0$ mV. (d) Globally optimal fitted results of the G maps, showing consistent asymmetries with (b). The black and white dashed crossed lines shown on the maps denote the conditions when ϵ_F and ϵ_{BW} align with the source/drain levels, namely, the Fano and BW resonant conditions. The intersection points are degenerate points, and their V_g values are indicated by vertical dashed lines. (e) G - V_g curves extracted from (d) at $V_{sd} = 0$ mV, correspond to the transmission probability spectra: the total fitted curve is the sum of a symmetrical BW curve, an asymmetrical Fano curve, and a constant off-resonant value.

TABLE I. Fitting parameters of the devices.

Device	1	2	3
Molecule	DPSBF	DPSBF	DPFO
Side group	Biphenyl	Biphenyl	Oxygen
Γ_F	6.79 ± 0.35 meV	2.86 ± 0.21 meV	4.80 ± 0.07 meV
Γ_{BW}	11.91 ± 0.64 meV	5.78 ± 0.45 meV	9.91 ± 0.49 meV
A_F	0.093 ± 0.0022	0.070 ± 0.0038	0.019 ± 0.0031
A_{BW}	0.299 ± 0.017	0.227 ± 0.0093	0.104 ± 0.012
A_{off}	-0.057 ± 0.0017	-0.053 ± 0.022	-0.012 ± 0.011
$\epsilon_F - \epsilon_{BW}$	8.04 ± 0.36 meV	6.26 ± 0.33 meV	-6.90 ± 0.28 meV
q	0.374 ± 0.013	-0.385 ± 0.007	1.87 ± 0.022

probability: A_F , A_{BW} , and A_{off} ; the Fano and BW resonant widths in transmission probability: Γ_F and Γ_{BW} ; the distance between the Fano and BW resonant levels: $\epsilon_s - \epsilon_b = \epsilon_F - \epsilon_{BW}$; the Fano asymmetry factor: q .

In addition, we perform experiments at different temperatures to investigate the temperature response of the Fano interference. Figure 2(a) shows the difference between G at 12 and 3 K ($G|_{12K} - G|_{3K}$). It can be found that the value of G increases with the temperature in the Fano region (red color), distinctly different from that in the BW region (blue color), strongly confirming the existence of distinct resonant modes. We then calculate the theoretical results of G at 9 and 12 K when all the transmission parameters are the same as those at 3 K. The theoretical $G|_{12K} - G|_{3K}$ [Fig. 2(b)] is in good agreement with the

experimental results in Fig. 2(a). The origin of the positive temperature response of G near the Fano region can be explained by the evolution of the dip-dominated Fano line shape.

As shown in Fig. 2(c), the dip-dominated Fano line shape becomes shallower when the temperature increases, resulting in an enhancement of G at the degenerate point. Moreover, the values of G at the Fano degenerate point (G_F) exhibit a linear response with T^2 [Fig. 2(d)]. This square law indicates a preserved interference mechanism, which means that the temperature response in G is mainly due to the variation of the Fermi-Dirac distribution functions of the gold electrodes⁵⁴ (see the discussion in Sec. 2.3 of the supplementary material).

We then analyze the mechanism of this Fano interference behavior. Previous studies have proposed a transport model to describe the Fano interference in the molecular junction with a long backbone and a side group.³⁴ However, the Fano form of this model only presents a dip-peak profile without a q factor, making it difficult to clearly characterize the features of the interfered states. Inspired by the studies of mesoscopic electronic Fano interference,^{23–32} we consider a finite coupling between the side group and the leads, thus introducing the q factor into the form that relates to the relative intensities and phases of the two transmission pathways. The detailed derivation of our model and the comparison between the models are provided in Sec. 3.1 of the supplementary material.

Here, we briefly introduce our model to characterize the features of the interfered states and the coupling configurations of the device. As shown in Fig. 3(a), the molecular backbone directly couples to the left and right leads, described by the coupling strength c_b (in energy unit). In contrast, the side group does not directly couple to the leads

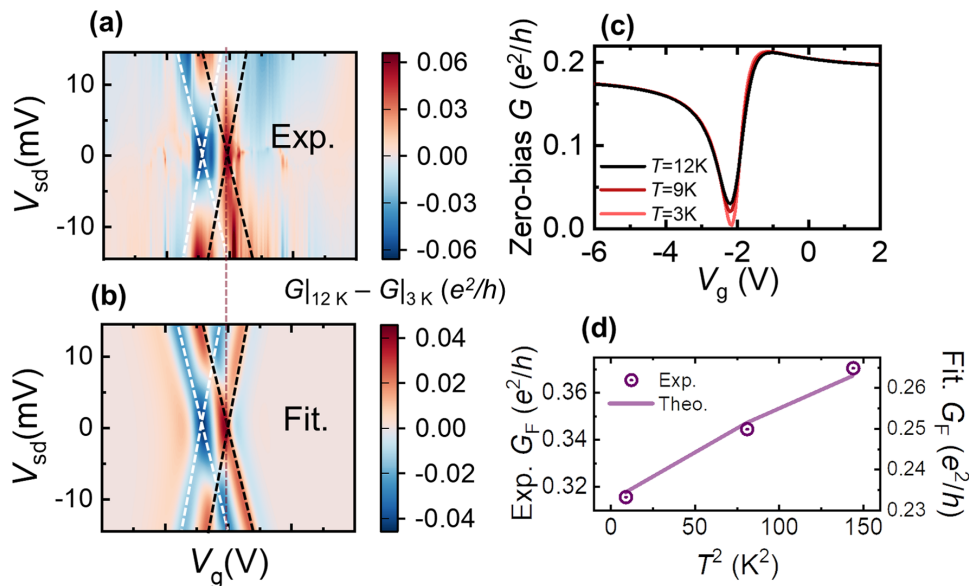


FIG. 2. Temperature response. (a) The difference between the experimental G at 12 and 3 K ($G|_{12K} - G|_{3K}$). The regions in red on the maps indicate the value at 12 K is larger than that at 3 K, while those in blue mean it is smaller. The BW crossing is located in the blue region, and the Fano crossing is located in the red region. (b) The theoretical map of ($G|_{12K} - G|_{3K}$) when τ remains invariant, showing consistent distribution with (a). (c) Zero-bias $G - V_g$ curves of the Fano component at different temperatures, exhibiting a shallower dip-dominated Fano line shape when the temperature increases. (d) The experimental and theoretical values of G at the Fano degenerate point (G_F) are plotted against the temperature squared T^2 . The linear relation between G and T^2 indicates the variation of Fermi-Dirac distribution functions of the gold electrodes when the temperature increases, but the transmission parameters remain invariant.

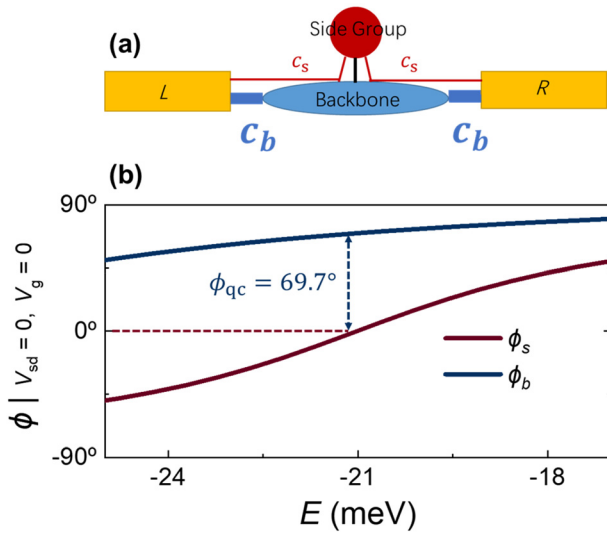


FIG. 3. Mechanism of Fano interference. (a) Models of the device. The states on the backbone and side group contribute to a transmission pathway. The backbone state has direct couplings c_b to the left and right leads, while the side state has indirect couplings c_s to the leads by the way of the backbone. (b) Transmission phases plotted against the energy for the side group (ϕ_s) and the molecular backbone (ϕ_b) obtained from the interferometry when $V_g = 0$ and $V_{sd} = 0$.

but can establish indirect couplings c_s to the leads by the way of the backbone. It is natural that $c_b > c_s$, corresponding to the charge state contributed by the backbone more sufficiently hybridized with the leads than that is contributed by the side group. This makes the transmission pathway through the backbone state tends to be a quasi-continuous state with a larger intensity, a wider broadening, and a less sensitive phase-energy response than that through the side state.

QI between such a pair of quasi-continuous and discrete states produces Fano resonance in the transmission spectrum as the forms of Eq. (1).⁵⁵ The positions and widths of the resonances are determined by the levels and broadening of the side and backbone states: $\epsilon_F - \epsilon_{BW} = \epsilon_s - \epsilon_b$, $\Gamma_{BW} = \Gamma_b$, and $\Gamma_F = \Gamma_s$. The Fano q factor describes the relative intensity of the discrete state and the continuum. Here, combined with the resonant widths and coefficients, it can be used to characterize the relative strength of the backbone-lead and side-lead couplings $\left(\frac{c_b}{c_s}\right)^4 = \frac{A_{BW}\Gamma_{BW}^2}{A_F\Gamma_F^2q^2}$, and the phase difference at the Fano resonant level: $\phi_b - \phi_s|_{E=\epsilon_s} = \arcsin \frac{A_F}{A_{BW}} \frac{1}{\left(\frac{\epsilon_F - \epsilon_{BW}}{\Gamma_F/2}\right)^2 + 1}$.

The backbone state has a larger broadening than the side one, agreeing with the quasi-continuous property. The energy level of the side state is higher than the backbone state in device 1. The value of $\left(\frac{c_b}{c_s}\right)^4$ is 70.4, indicating that the backbone-lead coupling is much stronger than the side-lead coupling. The phases-energy dependences of the transmission pathways in the range $(\epsilon_s - \Gamma_s/2, \epsilon_s + \Gamma_s/2)$ are plotted in Fig. 3(b), and one can see that the phase of the backbone pathway changes slower than the side pathway, also agreeing with the quasi-continuous property. The value of $\phi_b - \phi_s|_{E=\epsilon_s} = 69.7^\circ$ is just the phase of quasi-continuous state ϕ_{qc} when $\phi_s|_{E=\epsilon_s}$ is set to be zero.

The value of $\left(\frac{c_b}{c_s}\right)^4$ is 90.8 in device 2 and 6.87 in device 3. The value of $\phi_b - \phi_s|_{E=\epsilon_s}$ is 65.2° in device 2 and 46.4° in device 3. One

can see the results in devices 1 and 2 are relatively close to each other, while those in device 3 are significantly different. This is caused by the different side groups. In devices 1 and 2, the relatively large biphenyl side group in the DPSBF molecule contributes to a relatively independent side state from the backbone one. While in device 3, the small oxygen side group is closely attached to the backbone one. The side and backbone pathways are relatively separated in devices 1 and 2, while are relatively overlapped in device 3. Therefore, the values of $\left(\frac{c_b}{c_s}\right)^4$ and $\phi_b - \phi_s|_{E=\epsilon_s}$ that reflect the difference between the side and backbone pathways are larger in devices 1 and 2 than in device 3.

We implement first principles calculations (see further details of the calculation setting that are shown in Sec. 4 of the [supplementary material](#)) to understand the mechanism of the Fano interference phenomena and the characterized features in depth. We first investigate the molecular orbital characteristics of the bare molecule, shown in Fig. 4(a), with a focus on the levels closest to the Fermi energy of the gold leads. The lowest unoccupied molecular orbital (LUMO) level contributes to a quasi-continuous state that extends from one nitrogen anchor to the other one through a π state of the molecular backbone, while the LUMO + 2 level contributes to a discrete state that concentrates on the biphenyl side group. These correspond to a quasi-continuous transmission path with a large broadening Γ_b and a strong coupling c_b , than the side one. Although these two states are not neighbored to each other for the bare molecule, they can be closed enough to induce Fano interference when the molecule is connected into the junction due to the hybridization of the states.

We then perform NEGF-DFT simulations to assess the conductance within the device architectures illustrated in Fig. 4(b). We calculate the transmission spectrum of the device shown in Fig. 4(c) in which the dashed box marks the range related to the Fano interference we concern about. Integrating the calculated spectrum, we obtain the calculated zero-bias conductance as the function of the gate voltage, plotted in Fig. 4(d). This result shows an asymmetrical curve that aligns finely with the experimental result depicted in Fig. 1(c). The result is decomposed using Eq. (1), corresponding to the curves displayed in Fig. 4(e) with the parameters,

$$\Gamma_F = 4.243 \text{ meV}, \quad \Gamma_{BW} = 4.243 \text{ meV}, \\ \epsilon_F - \epsilon_{BW} = 2.55 \text{ meV}, \quad \text{and} \quad q = 0.803.$$

The relative positions of the BW and Fano components and the magnitudes of the q factors show a high degree of consistency with the experimental data.

In summary, we construct SMTs based on the molecule with a long backbone and a side group to gate Fano interference. By applying bias and gate voltages, we observe noncentrosymmetrical patterns of the differential conductance, which are finely fitted by ordinary Fano formula with the q factor. The experiments in different temperatures and different devices prove the robustness and reproducibility of such behavior. Based on a promotion of the previously reported transport model, the mechanism can be interpreted by the QI between a quasi-continuous transmission pathway through the backbone and a discrete transmission pathway through the side group. The q factor and other parameters help us to characterize the features of the interfered states and the coupling configurations. First principles calculations confirm the existence and features of the interfered states and prove that these

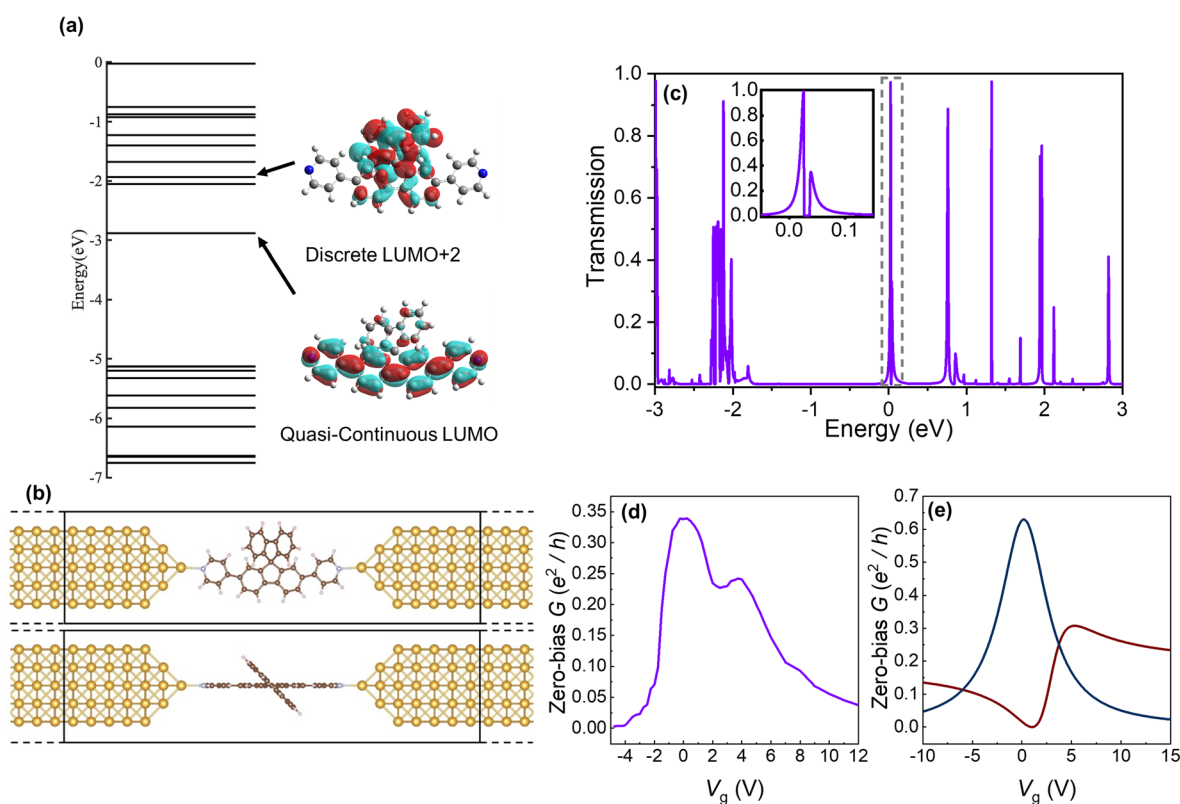


FIG. 4. The corroboration of Fano interference by first principles calculations. (a) Energy levels of the bare DPSBF molecule, and the spatial distribution of the states involving Fano interference. (b) Schematic of the simulated device. (c) Calculated transmission spectrum of the device. The range related to the Fano interference is marked by the dashed box, whose details are illustrated as the inset. (d) Calculated zero-bias conductance G as the functions of the gate voltages V_g . (e) BW and Fano components of fitted calculated conductance using Eq. (1) as the functions of the gate voltages V_g .

states can induce the asymmetrical Fano signals we observe in the experiments. As a result, our findings demonstrate an essential type of QI in three-terminal molecular devices, showing an instrumental method to observe, manipulate, and utilize the QI effect at the ultra-miniatured scale.

See the [supplementary material](#) for the preparation of the molecules and the devices, the derivation of the transport model, the details of the data fitting, the differential conductance data of devices 2 and 3, and the methods for the first principles calculations.

This work was supported by the National Key R&D Program of China (Grant Nos. 2022YFA1402404 and 2018YFE0202700), the National Natural Science Foundation of China (Grant Nos. 92161201, T2221003, 12104313, 12422410, 12104221, 12104220, 91961101, 12025404, 12004174, 62274085, 61822403, 11874203, and 11974422), the China Postdoctoral Science Foundation (Grant No. 2022M722191), the Strategic Priority Research Program of the Chinese Academy of Sciences (Grant No. XDB30000000), Department of Science and Technology of Guangdong Province (No. 2021QN02L820), Shenzhen Natural Science Fund (the Stable Support Plan Program 20220810161616001), and the Research Funds of Renmin University of China (Grant Nos. 22XNKJ30 and 21XNH090).

AUTHOR DECLARATIONS

Conflict of Interest

The authors have no conflicts to disclose.

Author Contributions

Yiping Ouyang, Rui Wang, Zewen Wu, Deping Guo, and Yang-Yang Ju contributed equally to this work.

Yiping Ouyang: Data curation (lead); Investigation (equal); Writing – original draft (lead). **Rui Wang:** Data curation (equal); Investigation (equal); Writing – original draft (equal). **Zewen Wu:** Data curation (equal); Investigation (equal). **Deping Guo:** Data curation (equal); Investigation (equal). **Yang-Yang Ju:** Investigation (equal); Resources (equal). **Jun Chen:** Data curation (supporting); Investigation (supporting); Writing – original draft (supporting). **Minhao Zhang:** Conceptualization (equal); Data curation (equal); Supervision (equal); Writing – original draft (equal); Writing – review & editing (equal). **Danfeng Pan:** Resources (equal). **Xuecou Tu:** Resources (equal). **Shuai Zhang:** Conceptualization (equal). **Lin Kang:** Resources (supporting). **Jian Chen:** Conceptualization (equal). **Peiheng Wu:** Resources (supporting). **Xuefeng Wang:** Conceptualization (equal). **Jianguo Wan:** Conceptualization (equal). **Wei Ji:** Data curation

(equal); Supervision (equal); Writing – review & editing (equal). **Xianghua Kong:** Data curation (equal); Supervision (equal); Writing – review & editing (equal). **Yuan-Zhi Tan:** Conceptualization (equal); Resources (equal); Supervision (equal); Writing – review & editing (equal). **Fengqi Song:** Conceptualization (equal); Data curation (equal); Funding acquisition (equal); Supervision (equal); Writing – original draft (equal); Writing – review & editing (equal).

DATA AVAILABILITY

The data that support the findings of this study are available from the corresponding authors upon reasonable request.

REFERENCES

- P. Gehring, J. M. Thijssen, and H. S. J. van der Zant, *Nat. Rev. Phys.* **1**(6), 381–396 (2019).
- J. Liu, X. Huang, F. Wang, and W. Hong, *Acc. Chem. Res.* **52**(1), 151–160 (2019).
- S. V. Aradhya and L. Venkataraman, *Nat. Nanotechnol.* **8**(6), 399–410 (2013).
- C. J. Lambert, *Chem. Soc. Rev.* **44**(4), 875–888 (2015).
- F. Evers, R. Korytár, S. Tewari, and J. M. van Ruitenbeek, *Rev. Mod. Phys.* **92**(3), 035001 (2020).
- C. M. Guédon, H. Valkenier, T. Markussen, K. S. Thygesen, J. C. Hummelen, and S. J. van der Molen, *Nat. Nanotechnol.* **7**(5), 305–309 (2012).
- S. Ballmann, R. Härtle, P. B. Coto, M. Elbing, M. Mayor, M. R. Bryce, M. Thoss, and H. B. Weber, *Phys. Rev. Lett.* **109**(5), 056801 (2012).
- H. Vazquez, R. Skouta, S. Schneebeli, M. Kamenetska, R. Breslow, L. Venkataraman, and M. S. Hybertsen, *Nat. Nanotechnol.* **7**(10), 663–667 (2012).
- M. H. Garner, H. Li, Y. Chen, T. A. Su, Z. Shangguan, D. W. Paley, T. Liu, F. Ng, H. Li, S. Xiao, C. Nuckolls, L. Venkataraman, and G. C. Solomon, *Nature* **558**(7710), 415–419 (2018).
- D. Z. Manrique, C. Huang, M. Baghernejad, X. Zhao, O. A. Al-Owaedi, H. Sadeghi, V. Kaliginedi, W. Hong, M. Gulcur, T. Wandlowski, M. R. Bryce, and C. J. Lambert, *Nat. Commun.* **6**(1), 6389 (2015).
- C. Tang, J. Zheng, Y. Ye, J. Liu, L. Chen, Z. Yan, Z. Chen, L. Chen, X. Huang, J. Bai, Z. Chen, J. Shi, H. Xia, and W. Hong, *iScience* **23**(1), 100770 (2020).
- X. Liu, S. Sangtarash, D. Reber, D. Zhang, H. Sadeghi, J. Shi, Z.-Y. Xiao, W. Hong, C. J. Lambert, and S.-X. Liu, *Angew. Chem. Int. Ed.* **56**(1), 173–176 (2017).
- Y. Li, M. Buerkle, G. Li, A. Rostamian, H. Wang, Z. Wang, D. R. Bowler, T. Miyazaki, L. Xiang, Y. Asai, G. Zhou, and N. Tao, *Nat. Mater.* **18**(4), 357–363 (2019).
- J. Bai, A. Daaoub, S. Sangtarash, X. Li, Y. Tang, Q. Zou, H. Sadeghi, S. Liu, X. Huang, Z. Tan, J. Liu, Y. Yang, J. Shi, G. Mészáros, W. Chen, C. Lambert, and W. Hong, *Nat. Mater.* **18**(4), 364–369 (2019).
- B. Huang, X. Liu, Y. Yuan, Z.-W. Hong, J.-F. Zheng, L.-Q. Pei, Y. Shao, J.-F. Li, X.-S. Zhou, J.-Z. Chen, S. Jin, and B.-W. Mao, *J. Am. Chem. Soc.* **140**(50), 17685–17690 (2018).
- C. Tang, L. Huang, S. Sangtarash, M. Noori, H. Sadeghi, H. Xia, and W. Hong, *J. Am. Chem. Soc.* **143**(25), 9385–9392 (2021).
- S. Soni, G. Ye, J. Zheng, Y. Zhang, A. Asyuda, M. Zharnikov, W. Hong, and R. C. Chiechi, *Angew. Chem. Int. Ed.* **59**(34), 14308–14312 (2020).
- A. Vezzoli, I. Grace, C. Brooke, K. Wang, C. J. Lambert, B. Xu, R. J. Nichols, and S. J. Higgins, *Nanoscale* **7**(45), 18949–18955 (2015).
- K. Wang, A. Vezzoli, I. M. Grace, M. McLaughlin, R. J. Nichols, B. Q. Xu, C. J. Lambert, and S. J. Higgins, *Chem. Sci.* **10**(8), 2396–2403 (2019).
- C. Wang, M. R. Bryce, J. Gigon, G. J. Ashwell, I. Grace, and C. J. Lambert, *J. Org. Chem.* **73**(13), 4810–4818 (2008).
- M. Camarasa-Gómez, D. Hernangómez-Pérez, M. S. Inkpen, G. Lovat, E. D. Fung, X. Roy, L. Venkataraman, and F. Evers, *Nano Lett.* **20**(9), 6381–6386 (2020).
- U. Fano, *Phys. Rev.* **124**(6), 1866–1878 (1961).
- A. E. Miroshnichenko, S. Flach, and Y. S. Kivshar, *Rev. Mod. Phys.* **82**(3), 2257–2298 (2010).
- V. Madhavan, W. Chen, T. Jamneala, M. F. Crommie, and N. S. Wingreen, *Science* **280**(5363), 567–569 (1998).
- J. Göres, D. Goldhaber-Gordon, S. Heemeyer, M. A. Kastner, H. Shtrikman, D. Mahalu, and U. Meirav, *Phys. Rev. B* **62**(3), 2188–2194 (2000).
- K. Kobayashi, H. Aikawa, S. Katsumoto, and Y. Iye, *Phys. Rev. Lett.* **88**(25), 256806 (2002).
- W. Yi, L. Lu, H. Hu, Z. W. Pan, and S. S. Xie, *Phys. Rev. Lett.* **91**(7), 076801 (2003).
- J. Kim, J.-R. Kim, J.-O. Lee, J. W. Park, H. M. So, N. Kim, K. Kang, K.-H. Yoo, and J.-J. Kim, *Phys. Rev. Lett.* **90**(16), 166403 (2003).
- B. Babić and C. Schönenberger, *Phys. Rev. B* **70**(19), 195408 (2004).
- L. Gao, W. Ji, Y. B. Hu, Z. H. Cheng, Z. T. Deng, Q. Liu, N. Jiang, X. Lin, W. Guo, S. X. Du, W. A. Hofer, X. C. Xie, and H. J. Gao, *Phys. Rev. Lett.* **99**(10), 106402 (2007).
- P. Gehring, H. Sadeghi, S. Sangtarash, C. S. Lau, J. Liu, A. Ardavan, J. H. Warner, C. J. Lambert, G. A. D. Briggs, and J. A. Mol, *Nano Lett.* **16**(7), 4210–4216 (2016).
- K. Hong and W. Y. Kim, *Angew. Chem.-Int. Ed.* **52**(12), 3389–3393 (2013).
- M. L. L. D. Guevara, F. Claro, and P. A. Orellana, *Phys. Rev. B* **67**(19), 195335 (2003).
- T. A. Papadopoulos, I. M. Grace, and C. J. Lambert, *Phys. Rev. B* **74**(19), 193306 (2006).
- C. M. Finch, V. M. García-Suárez, and C. J. Lambert, *Phys. Rev. B* **79**(3), 033405 (2009).
- A. Kormányos, I. Grace, and C. J. Lambert, *Phys. Rev. B* **79**(7), 075119 (2009).
- S.-H. Ke, W. Yang, and H. U. Baranger, *Nano Lett.* **8**(10), 3257–3261 (2008).
- A. K. Ismael, I. Grace, and C. J. Lambert, *Phys. Chem. Chem. Phys.* **19**(9), 6416–6421 (2017).
- Z. Y. Mijbil, *Chem. Phys. Lett.* **716**, 69–75 (2019).
- A. Grigoriev, J. Sköldberg, G. Wendin, and Ž. Crljen, *Phys. Rev. B* **74**(4), 045401 (2006).
- Y. Zheng, P. Duan, Y. Zhou, C. Li, D. Zhou, Y. Wang, L.-C. Chen, Z. Zhu, X. Li, J. Bai, K. Qu, T. Gao, J. Shi, J. Liu, Q.-C. Zhang, Z.-N. Chen, and W. Hong, *Angew. Chem. Int. Ed.* **134**(40), e202210097 (2022).
- Y. Zheng, P. Duan, Y. Zhou, C. Li, D. Zhou, Y. Wang, L.-C. Chen, Z. Zhu, X. Li, J. Bai, K. Qu, T. Gao, J. Shi, J. Liu, Q.-C. Zhang, Z.-N. Chen, and W. Hong, *Angew. Chem. Int. Ed.* **61**(40), e202210097 (2022).
- C. R. Prindle, W. Shi, L. Li, J. Dahl Jensen, B. W. Laursen, M. L. Steigerwald, C. Nuckolls, and L. Venkataraman, *J. Am. Chem. Soc.* **146**(6), 3646–3650 (2024).
- B. Xu and J. Tao Nongjian, *Science* **301**(5637), 1221–1223 (2003).
- H. S. J. van der Zant, Y.-V. Kervennic, M. Poot, K. O'Neill, Z. de Groot, J. M. Thijssen, H. B. Heersche, N. Stühr-Hansen, T. Bjørnholm, D. Vanmaekelbergh, C. A. van Walree, and L. W. Jenneskens, *Faraday Discuss.* **131**(0), 347–356 (2006).
- K. Zhang, C. Wang, M. Zhang, Z. Bai, F.-F. Xie, Y.-Z. Tan, Y. Guo, K.-J. Hu, L. Cao, S. Zhang, X. Tu, D. Pan, L. Kang, J. Chen, P. Wu, X. Wang, J. Wang, J. Liu, Y. Song, G. Wang, F. Song, W. Ji, S.-Y. Xie, S.-F. Shi, M. A. Reed, and B. Wang, *Nat. Nanotechnol.* **15**(12), 1019–1024 (2020).
- Z. Bai, X. Liu, Z. Lian, K. Zhang, G. Wang, S.-F. Shi, X. Pi, and F. Song, *Chin. Phys. Lett.* **35**(3), 037301 (2018).
- H. Park, J. Park, A. K. L. Lim, E. H. Anderson, A. P. Alivisatos, and P. L. McEuen, *Nature* **407**(6800), 57–60 (2000).
- W. Liang, M. P. Shores, M. Bockrath, J. R. Long, and H. Park, *Nature* **417**(6890), 725–729 (2002).
- F. Borsoi, K. Zuo, S. Gazibegovic, R. L. M. Op het Veld, E. P. A. M. Bakkers, L. P. Kouwenhoven, and S. Heedt, *Nat. Commun.* **11**(1), 3666 (2020).
- W. R. Lee, J. U. Kim, and H. S. Sim, *Phys. Rev. B* **77**(3), 033305 (2008).
- A. C. Johnson, C. M. Marcus, M. P. Hanson, and A. C. Gossard, *Phys. Rev. Lett.* **93**(10), 106803 (2004).
- R. Landauer, *IBM J. Res. Dev.* **1**(3), 223–231 (1957).
- M. Paulsson and S. Datta, *Phys. Rev. B* **67**(24), 241403 (2003).
- Y. N. Lv, A. W. Liu, Y. Tan, C. L. Hu, T. P. Hua, X. B. Zou, Y. R. Sun, C. L. Zou, G. C. Guo, and S. M. Hu, *Phys. Rev. Lett.* **129**(16), 163201 (2022).